JOURNAL OF MATERIALS SCIENCE 15 (1980) 177–187

Fracture of a brittle composite: influence of elastic mismatch and interfacial bonding

ARUP K. KHAUND*, PATRICK S. NICHOLSON
Department of Metallurgy and Materials Science, McMaster University, Hamilton, Ontario, Canada

The influence of the presence or absence of elastic mismatch between the dispersed and matrix phases on local crack particle interactions in brittle composites is reported. The role of interfacial bond strength is also investigated in the presence of elastic stress concentrations. The optimum toughness possible for a brittle composite results when $G_i \leqslant G_m$, (G_i, G_m – elastic rigidity moduli for inclusion and matrix), and the interfacial bond strength is sufficient to allow plastic deformation of the dispersed phase. The dispersion of a ductile second phase with high interfacial bond strength but $G_i > G_m$, reduces effective crack/particle interactions. To increase the toughness in this case, weak interfacial bonding is necessary. Ultrasonic fractography was used to verify the local crack/particle interactions in detail.

1. Introduction

It has long been recognized that highly brittle ceramic materials possess many attractive properties. The serious drawback of these materials is their proneness to catastrophic failure under thermal shock and mechanical impact. The addition of a second phase influences their resistance to crack propagation (or toughness) and the following work shows that tough ceramics may be possible via multiphase composites. Earlier work [1, 2] investigated the influence of pseudoporosity (weak interfaces) on local crack/particle interactions. The present work illustrates the details of elastic mismatch/interfacial bonding in such interactions.

According to Griffith [3], during crack propagation in a brittle material, the energy demand curve is a straight line. The energy release curve, on the other hand, is a parabola. Crack instability occurs when the slopes of the two curves are equal. The implication is that "instability" (propagation) is assured in advance, once the crack is initiated [4]. In a single-phase homogeneous brittle material, since the energy demand is the same everywhere, the initiation and propagation of a crack coincide and fracture is instantaneous. In the development of "tough ceramics", the objective is to promote a stage of stable crack propagation. When crack arrestors are present in a brittle matrix, the energy-demand curve is non-linear [5]. Non-linearity arises from the ability of the second phase to stabilize a growing crack by requiring more energy to "clear" its obstacles [4].

Second-phase inclusions (including pores) of different elastic moduli and thermal expansivity than the matrix give rise to local stress concentrations in particulate composites [6, 7]. The nature of the interface between the second phase and matrix will also influence their fracture mechanical properties [8, 9]. Stett and Fulrath [10] investigated the mechanical strength of glass–nickel sphere systems. By oxidizing the nickel, they formed an interfacial bond of varying strength. They reported that the optimum bond strength depends upon the thickness of the oxide layer. However, they did not investigate the effect of the continuously varying bond strength on the fracture toughness properties. For systems where particles are dispersed in a glass matrix, several workers [11–14] have observed an increase in the effective fracture energy of the system over that for glass. Little is known of the local crack–

*Present address: Erie Technological Products of Canada Ltd, Trenton, Ontario, Canada.

0022–2461/80/010177–11$03.10/0 © *1980 Chapman and Hall Ltd.*

particle interactions in such composites and their influence on the overall toughening. In the present work, such interactions were studied via SEM microphotography and ultrasonic fractography. The bond strength in the systems studied was varied and conditions of maximum and minimum (~ 0) elastic mismatch were investigated.

In many materials, crack propagation does not proceed in a planar fashion. Abrupt changes in crack path lead to local reductions of the mechanical energy release rate and apparent increases in the fracture surface energy. In brittle particulate composites, mechanical energy can also be dissipated via local plastic deformation of particles ahead of the crack tip. Such was observed by Mendelson and Fine [15] for Fe in magnesiowustite. For this to occur, the bond strength between the second phase and the matrix must be equal to or greater than the matrix strength, and the crack path must not be altered by local elastic stress concentrations so as to avoid the associated particles. If weak interfaces exist in a multiphase material, it is conceivable that the region ahead of a crack may contain a decohesed zone. This will increase the fracture toughness of the material if the fracture area associated with such a zone is large. There is evidence of such zones in concrete [16], rocks [14], and partially stabilized zirconia [17, 18].

The formation of a large microcrack zone is unlikely in a glass–particulate composite; however, an equivalent mechanism, i.e. the decohesion of weakly-bonded particles, may be an important energy absorbing mechanism in the presence of elastic mismatch between the second phase and matrix. The crack front will be locally blunted when it intersects pores, weak interfaces, grain boundaries, etc., and the local stress distributions ahead of it will be altered.

The size of such a decohesed zone can be estimated [19]. For spherical obstacles, a part of the interface is always subject to a maximum normal stress so that all the partciles within such a zone should decohese to some extent. The contribution to fracture surface energy of zone formation is [19]:

$$\gamma_{\text{decohesed zone}} \simeq \tfrac{1}{2} N_A A_{TC} (\sigma_T a_0), \quad (1)$$

where, for the two-dimensional case, A_{TC} is the area of the critical decohesed zone, N_A the number of particles per unit area, σ_T the critical stress needed to decohese the interfaces, and a_0 the interatomic distance. For a random distribution of uniform spheres of radius r [20]:

$$N_A = \frac{3V_v}{2\pi r^2} \quad (2)$$

where V_v is the volume fraction of particles. From the treatment of the formation of microcracks in a ceramic matrix by Hoagland *et al.* [21]:

$$A_{TC} = 1.12 \left(\frac{K_{IC}}{\sigma_T}\right)^4. \quad (3)$$

Substituting Equations 3 and 2 into Equation 1, it follows that:

$$\gamma_{\text{decohesed zone}} = 0.84 \frac{K_{IC}^4 a_0}{\pi \sigma_T^3} \left(\frac{V_v}{r}\right). \quad (4)$$

This equation shows that, for constant r and V_v, the contribution of the decohesed zone will be a maximum for the weakest interfaces. This concept will also be tested in the present work.

There is substantial fractographic evidence [22–24] that a crack front changes shape as it approaches and as it intersects a second-phase particle. A model to describe this interaction was first conceived by Lange [25]. He proposed that the increased crack length associated with bowing could contribute significantly to the fracture energy of a brittle composite. A value for "line-energy" per unit crack length, T, was estimated by dividing the elastic strain energy associated with a semicircular crack, by its length. Thomson [26] has since point out, however, that this "tension" will depend critically on the crack shape. The Lange model ignores the influence of the particle stress field and resultant changes of crack shape. Such stress fields will exist when elastic or thermal mismatch exists between the inclusions and matrix. The particles themselves could contribute to the fracture resistance and mechanisms of particle cleavage or interfacial decohesion should also be included to understand the entire fracture process in such composites. Lange [25] investigated the fracture mechanical behaviour of glass/Al_2O_3 particulate composites and attributed the increased fracture energy to an increase in crack front length due to bowing. The elastic mismatch between the glass and Al_2O_3 is significant ($E_{Al_2O_3} \simeq 6E_{glass}$), but its influence was not considered. For the glass–partly–oxidized–Ni system, Stett and Fulrath [10] indicated that the stress concentrations due to the elastic mismatch give rise to Griffith flaws of length such as to degrade the composite strength. The inter-

action between these elastic fields and the crack-tip stress field was not studied. Evans [27] modified Lange's treatment, computing the elastic stored energy associated with different crack-shape configurations. He also ignored the obstacle's elastic stress field and failure mechanisms.

The stress field due to elastic or thermal mismatch between the particles and the matrix can alter the crack path. If the thermal expansion coefficients of the two phases are different, hydrostatic stresses will result [7]. With good bonding between the inclusion and matrix, these stresses will be stored as "residual stress". The stress field σ_{yy} (for Mode I opening) of an approaching crack will be influenced by this residual stress. In the present work, such stresses were eliminated by matching the thermal expansion coefficients of the glass and inclusions.

The elastic stress concentrations in an infinite matrix due to the presence of circular and spherical inclusions with different elastic constants to those of the matrix, were determined by Goodier [28], using linear elastic theory. For systems in which the rigidity modulus for the dispersed phase (G_i), is greater than that of the matrix (G_m), a stress maximum occurs in the radial component of the stress field (σ_{rr}) along the $\theta = 0^\circ$ (polar position) direction [29]. This stress concentration at the poles of the inclusion will influence the crack to avoid the particle, so minimizing interaction between the crack front and elastic-energy-absorbing second phase. There is also a compressive region in the radial component, σ_{rr}, near $\theta = 90^\circ$. The value of this compressive field is small, but it will decelerate an approaching crack front. The tangential component of stress, $\sigma_{\theta\theta}$, is tensile along $\theta = 90^\circ$, but is less than the applied stress in this case. For a pore, on the other hand, the maximum stress concentration occurs in the tangential component ($\sigma_{\theta\theta}$) of the stress system along $\theta = 90^\circ$, and the crack front is attracted to the pore.

An estimate of the change of local K_I (stress concentration factor) to (K_{new}), due to the presence of stress fields around cylindrical as well as spherical inclusions has been made using the concept of an "image stress" on the crack front due to the inclusion ahead of it [29]. It was shown that, if $K_{new} < K_I$, the velocity of the crack front will decrease as it approaches the inclusion. If $K_{new} > K_I$, the velocity of the crack front will increase as it approaches the inhomogeneity. Hence, the velocity of the crack front should locally decrease as it approaches a spherical well-bonded nickel inclusion in glass ($K_{new} < K_I$) and locally accelerate towards a pore ($K_{new} > K_I$ as $G_i = 0 < G_m$). Obviously, for such elastic stress concentrations to develop, good bonding is prerequisite.

Hence, depending on the value of the elastic properties of the second phase and the matrix, the crack-front velocity and shape and the crack path will change. These interactions were studied in the present work for glass–partly-oxidized-nickel ($G_i > G_m$; variable bonding) and in glass–partly-oxidized-aluminium ($G_i = G_m$; good bonding) systems.

2. Materials and experimental details

Table I lists the compositions of the glasses and the dispersed particles with the relevant elastic and thermal coefficients. The expansivities of the glass and inclusions were closely matched to minimize thermal stress.

The raw materials for the glasses were dry mixed in a tumble mill, calcined at 700° C for 8 h, and then melted. They were fired for 10 h in a fireclay crucible at ~ 1450° C (S glass), and ~ 1050° C (M glass). Each was then cast into a graphite mould and ground up.

The nickel powder was in smooth spherical form. It was sieved to (− 100, + 140) mesh and oxidized 10 g at a time at 750° C using a wide-bottom alumina crucible. The particles were weighed before and after oxidation to determine the percentage weight gain. The aluminium particles (purity 99.9%: − 100, + 140 mesh) were also oxidized but the oxidation conditions were fixed at 450° C for 3 h. An average per cent weight gain of 0.57% was recorded.

Appropriate fractions of the glass and second phase particles were mixed for 24 h, placed in a graphite mould, and vacuum-hot-pressed into composite discs. The temperature was raised slowly to ~ 300° C (S glass composites) and a small pressure (0.3 MPa) applied. The temperature was then raised to 675° C. The final densification pressure (8.0 MPa) was applied slowly for ~ 30 min. The hot-pressed samples were finally annealed at 520° C for 4 h. The pressing temperature for the M glass composite was 500° C and an initial load (0.3 MPa) was applied at ~ 200° C. Hot-pressed samples < 95% theoretical density were rejected.

TABLE I

Composite systems	Glass compositions (% WF)	Second phases	Volume fraction (Λ)	Particle size	α_m $\times 10^{-6}$ ($^\circ C^{-1}$)	α_i* $\times 10^{-6}$ ($^\circ C^{-1}$)	E_m (10^6 psi)†	E_i (10^6 psi)	V_m	V_i	ρ_m	ρ_i
I	55% SiO_2 15% Al_2O_3 30% Na_2O (S glass)	Partly oxidized Ni particles; oxidation time: 0, 30, 60, 90, 120 min	7% and 3% at 30, 60, 90, 120 min 0%, 7%, 15%, 20% at 30 min	−100, + 100 mesh size	13.8	~ 13.9	9.8	30	.2	.40	2.47	8.9
II	50% SiO_2 37% Na_2O 7% Al_2O_3 6% Li_2O (M glass)	Partly oxidized aluminium; oxidation time: 180 min	0%, 7%, 15%, 20%	−100, + 100 mesh size	~ 16.0	~ 16.0	9.1	~ 9.0	.2	.40	2.47	2.74

*α = thermal expansion coefficient; E = Young's modulus; V = volume fraction; ρ = density.
Subscripts: m = matrix; i = inclusion.
†10^3 psi = 6.89 N mm^{-2}.

A double cantilever beam (DCB) testing method was used to determine the G_{IC} values of the composites. Prior to testing, G_{IC} values for standard Corning 7740 Pyrex glass were determined. Values within 10% of those in the literature were obtained. The fracture strength of the composites was determined on machined 6 m x 10 mm x 40 mm samples, using a self-aligning four-point bend rig. The fractured surfaces were viewed under an SEM for fractographic evidence of crack–particle interaction.

The experimental arrangement for the ultrasonic modulation of DCB specimen fracture surfaces has been described elsewhere [30]. A transmitter of range 100 to 1000 W was used. For the glass samples, an intensity of 0.1 to 0.2 W mm^{-2} gave acceptable results.

3. Results

The fracture toughness (G_{IC}) values of the S glass–nickel composites for varying oxidation times are shown in Fig. 1. These results show a fracture toughness maximum for the 30 min oxidized composite. The fracture toughness values, after 120 min, were lower (even after experimental error) than for no oxidation (no chemical bonding).

Plots of G_{IC} for glass–aluminium as a function of volume-fraction second phase are shown in Fig. 2. There is a substantial increase of G_{IC} (~ 10 J m^{-2} to ~ 520 J m^{-2}) for the 20 vol % composite. By comparison, the S glass–oxidized nickel composites showed an increase from ~ 10 J m^{-2} to ~ 50 J m^{-2} for 15 vol % fraction (Fig. 2). The inherent toughness of nickel particles is higher than aluminium and these results demonstrate that the toughness of the nickel was not utilized.

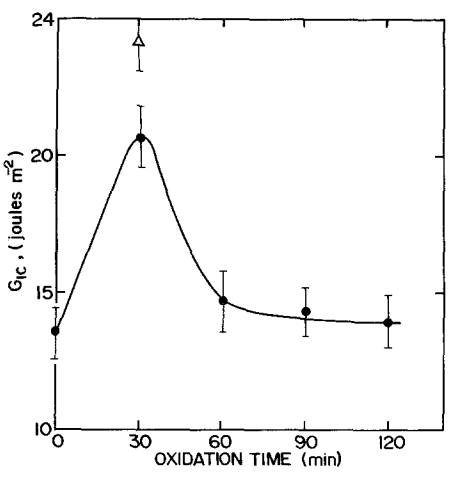

Figure 1 ○, plot of G_{IC} versus oxidation time for partially oxidized Ni (vol. fraction = 7%). Δ, plot of G_{IC} of "special particulate composite" (see text).

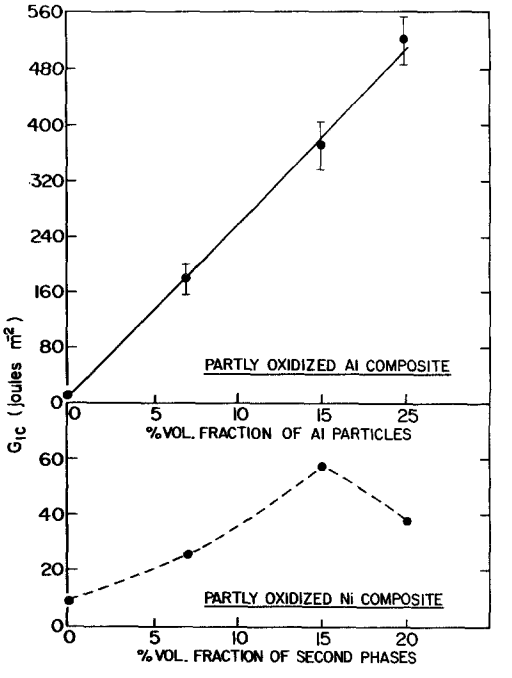

Figure 2 Plot of G_{IC} versus volume fraction for composites at given oxidation times (Ni = 30 min; A = 180 min).

The occurrence of a maximum in the G_{IC} values is not new. Such has been observed in several polymeric composite systems [30] and is generally attributed to the linkage of small flaws initiated at individual inclusions to form one single large flaw.

Fracture strength versus oxidation time for a 7 vol % nickel–S glass composite is shown in Fig. 3. The strength values are, in general, lower than those of the glass. This can be attributed to the weak interfacial bond giving rise to flaws on load application [19].

A polished section of the S glass–120 min oxidized Ni is shown in Fig. 4. The oxide layer is evident. Figs. 5 and 6 show the fracture surface of a 7 vol % Ni composite for the cases of the strongest bond (oxidation time ~ 120 min) and the weakest bond (oxidation time ~ 30 min). For the strongest interface, the crack avoids the particles (Fig. 5) and passes through the matrix as a result of elastic stress concentrations at the

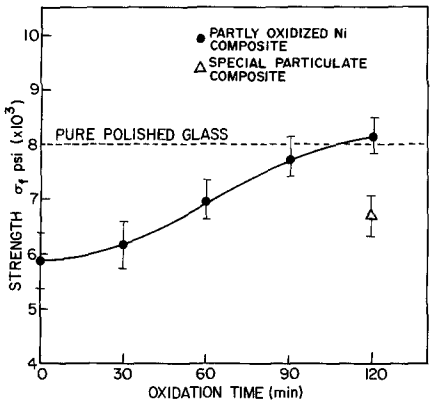

Figure 3 ○, plot of fracture strength of S glass–partly oxidized nickel composite as a function of oxidation time. Δ, strength value of "special particulate composite".

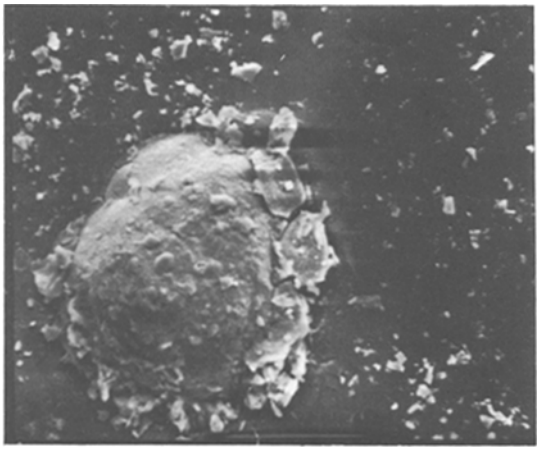

Figure 6 Fracture surface when bonding between particle and matrix is weak. The stress concentration at poles of the inclusion did not affect crack path.

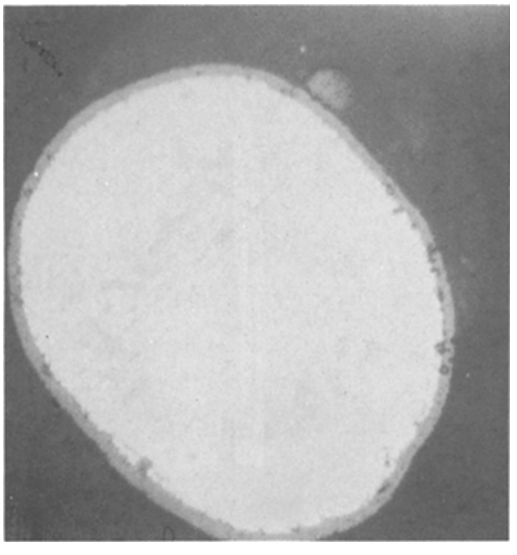

Figure 4 Polished section of 120 min oxidized nickel particles in nickel–S glass composite, × 540.

particle poles ($G_i > G_m$). Fig. 6, on the other hand, shows a completely decohesed interface, i.e. the stress component, σ_{yy}, at the crack tip decoheses the interface before the crack reaches it. On interfacial failure, the stress concentration at the poles reverts to the equator, assuring maximum interaction between the crack and the particle. No deformation of nickel is evident in either case.

The fracture surface of the glass–well-bonded aluminium composite is shown in Fig. 7. Large plastic deformation has been suffered by the particle. This plastic deformation is responsible for the observed increase of fracture toughness (× 50). Interfacial fracture around the deformed particles suggests that, after some particle deformation, the interface reaches a critical stress level and fractures. The crack path is unaltered and

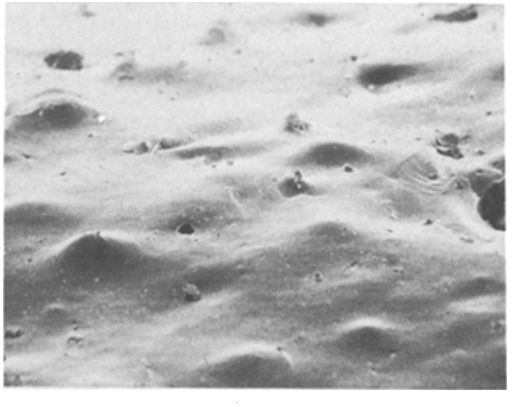

Figure 5 Observed crack path in glass–well-bonded Ni/NiO composite where effect of stress concentration is observed (120 min oxidation time).

Figure 7 Tilted image of failure of ductile (Al) particle in a glassy matrix (× 200).

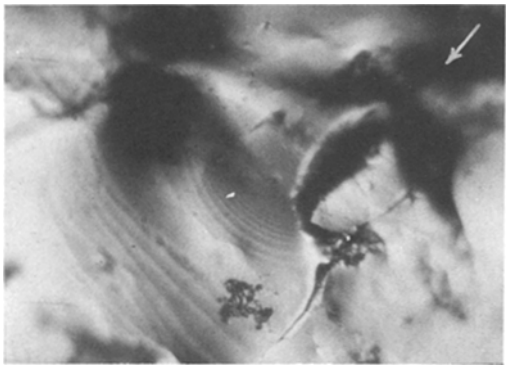

Figure 8 Crack bowing as shown by ripples between two (Ni) particles. Nickel particles were weakly bonded to the matrix. (30 min oxidation time, crack direction arrowed.)

shows no preferred propagation direction. This results from the absence of elastic stress concentrations in this composite.

Local crack–particle interactions were studied by ultrasonic fractography in S glass–partly oxidized nickel composites in which the interfacial strength was continuously varied. The interaction for a 30 min oxidized composite is shown in Fig. 8. The bowing of the crack between two nickel particles is evident. As the crack breaks away from the particles, its local velocity increases (increased ripple spacing). The extent of bowing is higher than for the unbonded non-oxidized Ni composite [1], i.e. the maximum angle of bowing at breakaway was $\sim 25^\circ$, whereas that for the unbonded composite was $\sim 13^\circ$. Fig. 9 shows the crack bowing around a 60 min oxidized particle. The bowing angle in this case was $\sim 32^\circ$. Fig. 10 shows interfacial decohesion and concurrent crack-

Figure 9 Crack bowing around a nickel particle intermediately bonded to glass. (60 min oxidation time, crack direction arrowed.)

Figure 10 Ni/NiO interfacial failure gives "pseudoporosity" and crack interacts with particle (crack direction arrowed).

front bowing. For the 60 and 90 min oxidation composites, the crack *avoided* the majority of particles. Fig. 9 illustrates the special case when the crack approaches the particle exactly along the equatorial plane. In this case, the equal deflection stress of either pole ensures the crack intersects the particle. In the 30 min oxidized composite,

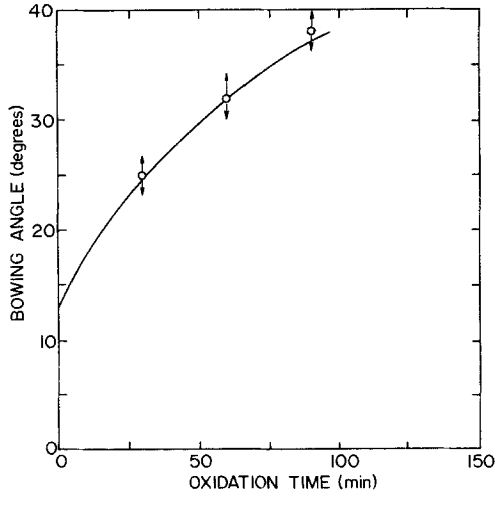

Figure 11 Plot of angle of bowing of crack front versus oxidation time.

the interfacial decohesion and consequent crack bowing are the main sources of increased crack resistance. A plot of the bowing angle (θ_m) versus oxidation time is shown in Fig. 11.

The nature of interaction between the crack front and the inclusion changes completely when the interfacial bond is sufficient to resist decohesion by the stress component (σ_{yy}) ahead of the crack tip. In this case, the crack approaches the particle and when near it, reacts to the radial stress concentration (θ_{rr}) at the poles of the inclusion. It changes its plane of propagation and bypasses the inclusion. This phenomenon is illustrated in Fig. 12. The sudden increase of crack velocity under the influence of the polar stress is clearly shown. The crack front jumps to the pole of the particle. Prior to this, the equatorial compressive stress decelerates the crack as evidenced by the ripple spacing. The change of crack velocity as a function of the apparent distance from the pole of the inclusion (measured from the ripple spacing and the u.s.* frequency) is shown in Fig. 13. The velocity decreases from 6 m sec^{-1} to ~ 0.8 m sec^{-1} on approach and jumps up to ~ 20 m sec^{-1} when the crack front is near the inclusion.

Ultrasonic fractography was impossible in the case of the glass–Al composites. The fracture surfaces were very rough, rendering identification of ultrasonic ripples impossible. It can be speculated that the plastic deformation of the Al particles must have been accompanied by multiple crack-path changes as the local stress state in the matrix glass changed in response to the inhomogeneous deformation of the Al particles.

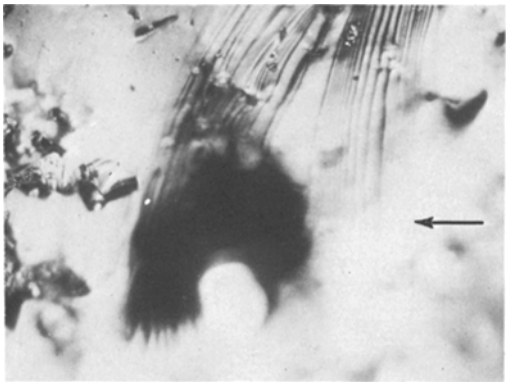

Figure 12 Attraction of crack front towards the polar stress concentration in a good bonding case. (120 min oxidation time, crack direction arrowed.)

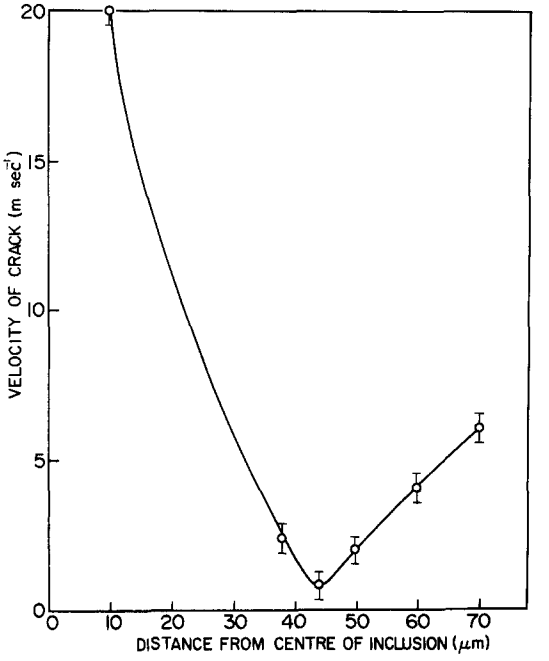

Figure 13 Plot of change of velocity of crack front in near vicinity of inclusion. The crack front approaches inclusion and finally avoids it.

4. Discussion

The ultrasonic fractographic evidence and the general SEM fracture surface features indicate that elastic mismatch has a definite effect on local crack–particle interactions in particulate composites, and may considerably influence their toughness. This effect is manifested by the directing of the crack path. On approaching a pore, the isostress contours are such that the crack feels a $\sigma_{\theta\theta}$ component along the equatorial plane of the inclusion ($\sim 3\sigma_{applied}$) attracting it to the pore. For glass–well-bonded nickel, the crack deflects to the pole and the only additional contribution to the fracture toughness is the increased fracture surface area due to the alteration of crack path (Fig. 5).

In the glass–aluminium composite, due to the absence of elastic mismatch between the glass and aluminium, no such stress concentrations occur and the crack front is undisturbed on approaching the inclusion. It meets the particle, and, with a sufficiently strong interfacial bond, plastically deforms it, utilizing some of the toughness of the second phase (Fig. 7).

These results are of interest as they show that ductile dispersions in a brittle matrix do not necessarily increase the composite toughness

* u.s. = ultrasonic.

even when interfacial bonding is adequate. The elastic properties of the inclusions must be such that $G_i \leqslant G_m$. Weak interfaces are more effective in improving the fracture toughness when $G_i > G_m$.

When a crack front approaches a weak interface, the normal stress component σ_{yy} in front of the crack decoheses the interface, creating a "pseudopore". The crack is attracted to this pseudopore by the increased $\sigma_{\theta\theta}$ component. Once it cuts the pseudopore, the crack front is locally blunted and a higher stress is required for its breakaway. When a weak but bonded interface is present, there will be an additional contribution associated with the process of decohesion. Hence, the total change in fracture toughness for such composites is composed of two contributions, i.e.

$$(\Delta\gamma)_{\text{weak interface}} = (\gamma)_{\text{decohesion zone}} + (\gamma)_{\substack{\text{shape change} \\ \text{because of blunting}}} \quad (5)$$

where γ is the fracture energy. Considering that decohesion occurs within a zone of the crack front, the form of Equation 4 indicates that, provided r and V_v are constant, the toughness contribution from a decohesed zone will be a maximum for the weakest interface. Comparison of G_{IC} values at 30 min oxidation time with those for 0 min oxidation time [18] for 7 vol % fraction, yields a value of 5 J m^{-2} for $\gamma_{\text{decohesion}}$. The value of γ_T in Equation 4 is difficult to calculate analytically for the case where chemical bonding exists. An attempt was made by Weirauch [32] to calculate the bonding energy (E) of a glass–metal interface involving purely mechanical adhesion. His results give that $E \equiv A_C DS$, where A_C is the total area of contact between glass and metal, D is the deformation of the metal, and S the yield strength of the metal. For the glass–Ni interface, substituting characteristic values for D and S, the bonding energy is comparable with the fracture energy of glass (~ 5 J m^{-2}) even when the broken area of contact, A_C, is 25% of the total area. Thus, in the case of weak adhesion, even after the crack front stress field partially decoheses the interface, there may be sufficient residual bonding to resist the motion of the propagating crack causing crack bowing and an additional contribution to the fracture energy. This kind of crack–particle interaction was observed in Fig. 10 where the unbroken part of the interface induced greater bowing of the crack front.

The extent of contribution of the second term can be discussed in terms of local crack bowing. When a crack front intersects a void, the stress distribution ahead of the crack is altered. Weiss [33] described the reduced stress ahead of such a crack front, i.e.

$$\sigma_{yy} = \sigma_A \left(\frac{4c}{\rho + 4r} \right) \quad (6)$$

where r is the radius of the pore, ρ the crack tip radius, c the crack length, and σ_A the applied stress.

For a crack interacting with a series of voids or decohesed particles, the value of σ_{yy} is locally reduced and this gives rises to a local variation in the fracture resistance. This is reflected by the bowing of the crack front around and between non-bonded or decohesed particles. The combination of these two processes gives rise to the maximum value of G_{IC} for the 30 min oxidation time interface. Beyond this time, the interface becomes too strong for decohesion and the elastic deflection of the crack over the particles eliminates the operation of both these toughening mechanisms. The toughness therefore drops. It is observed to drop below the value for unoxidized spheres of Ni. This is to be expected as the pseudopore blunting contribution is also absent in the strong interface case.

A weak interface is not desirable in elastically matched composites if the inherent toughness of the second phase is to be utilized. This is the case for the M glass–aluminium composites, in which considerable deformation of the aluminium particles occurred before interfacial fracture. The total toughness of a particulate composite with a dispersion of high-toughness second phase of matching elastic modulus can be expressed approximately as:

$$(G_{IC})_{\text{total}} = V_m (G_{IC})_m + k V_f (G_{IC})_i \quad (7)$$

where $(G_{IC})_m$ and $(G_{IC})_i$ are the toughness of the matrix and inclusion, and V_m and V_f are their respective volume fractions. The value of the coefficient k depends on the strength of interfacial bond. $k = 1$ signifies optimum interfacial bonding. For the glass–aluminium composites, $(G_{IC})_{\text{total}} = 520$ J m^{-2} at $V_f = 0.2$ (Fig. 2), and $(K_{IC})_i = 9000$ J m^{-2}. This yields a value of $k \sim 0.3$, indicating that only partial

utilization of the Al toughness was possible because of the limited bond strength achieved.

Any detailed model of the interaction of a crack front with second-phase particles should include the effect of the crack acceleration/deceleration towards the inclusions. The models proposed by Lange [25] and Evans [27] neglect this. The ultrasonic fractographs show the breakaway crack shape is not semi-circular but semi-elliptical. Evans, using the variation principle, calculated the breakaway shape parameter $F(a/2C)$ (where a is the semi-major axis of the semi-ellipse at breakaway and $2C$ is the interparticle spacing). If the crack front is obstructed by an "impenetrable obstacle", $F(a/2C) = 1$. In the glass–well-bonded Ni composite, this optimum condition did not occur since the crack front avoided the particles and propagated entirely through the matrix. In the weakly bonded Ni case, $(F(a/2C) > 1)$, the crack front interacts with the pseudopore giving crack-bowing.

A special particulate composite was fabricated of S-glass and 7 vol % dispersion of nickel particles of 30 min oxidation (interface corresponding to optimum toughness) and 7 vol % nickel particles with 120 min oxidation time (corresponding to optimum fracture strength). The values of G_{IC} and fracture strength σ_f for this composite are shown as triangles (Δ) on Figs. 1 and 3, respectively. The fracture surface of this composite is shown in Fig. 14. It is evident that mixed mode fracture occurred, i.e. "humps" and "decohesed particles" are evident. The G_{IC} value was slightly higher than that for the 7 vol % dispersion of 30 min oxidation, indicating an additional contribution to G_{IC} from the additional 7 vol % well-bonded Ni particles. The strength values were, however, not improved over those of the well-bonded nickel case. This is attributable to the creation of flaws at the weak interfaces and the consequent reduction of strength. It is evident that good bonding of both dispersants is required if the strength is to be maintained.

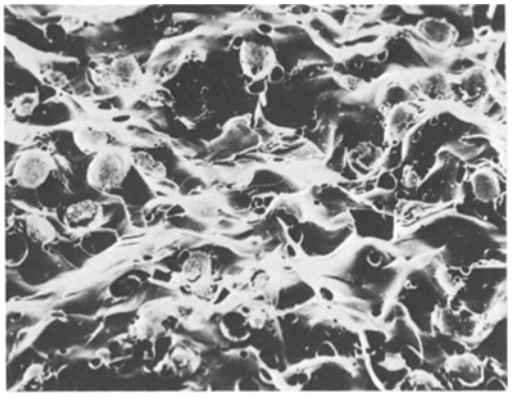

Figure 14 Mixed mode of fracture for well-bonded (120 min) and weakly bonded Ni particles (30 min) in the "special composite".

5. Conclusions

From this study, the following important points can be made:

(1) for significant toughening of a brittle composite by a dispersion of second phase, the inherent toughness of the second phase must be utilized;

(2) effective crack–particle interactions take place only when $G_i \leqslant G_m$ and when the interfacial bonding between the inclusion and matrix is strong. Otherwise, the crack path is altered towards the particle poles, eliminating interaction;

(3) elastic mismatch influences the local crack velocity on approaching an inclusion or pore;

(4) interfacial bonding plays a dual role in improving the toughness of particulate composites. When elastic mismatch is absent, stronger interfacial bonding effectively aids the utilization of the inherent toughness of the second phase. When elastic mismatch does exist, good interfacial bonding alters the path of the crack front to avoid the particles, so, in such composites, toughness improvement only results when weak interfacial bonding exists.

References

1. D. J. GREEN, P. S. NICHOLSON and J. D. EMBURY, *J. Mater. Sci.* **14** (1979) 1413.
2. *Idem, ibid.* **14** (1979) 1657.
3. A. A. GRIFFITH, *Phil. Trans. Roy. Soc. London* **221A** (1920) 163.
4. T. K. GUPTA, *J. Mater. Sci.* **2** (1974) 1585.
5. J. GLUKLICH, *J. Eng. Mech. Proc. ASCE* **89** (1962) 127.
6. J. N. GOODIER, *J. Appl. Mech.* **1** (1933) 39.
7. J. SELSING, *J. Amer. Ceram. Soc.* **44** (1961) 419.
8. D. P. H. HASSELMAN and R. M. FULRATH, *ibid* **50** (8) (1967) 395.
9. F. F. LANGE and K. C. RADFORD, *J. Mater. Sci.* **6** (1971) 197.
10. M. A. STETT and R. M. FULRATH, *J. Amer. Ceram. Soc.* **53** (1970) 5.
11. P. J. MALLICK and L. J. BROUTMAN, *Mater. Sci. Eng.* **18** (1975) 63.
12. P. HING, *Proc. Brit. Ceram. Soc.* **25** (1975) 13.
13. C. T. FORWOOD, *Phil. Mag.* **17** (1968) 657.
14. A. R. ROSENFIELD, G. T. HAHN and R. G.

HOAGLAND, *J. Roch. Mech.* 5 (1973) 77.
15. M. I. MENDELSON and M. E. FINE, *J. Amer. Ceram. Soc.* 57 (4) (1974) 154.
16. M. F. KAPLAN, Proceedings of the International Conference on Structure of Concrete, Paper D7, London (1965).
17. G. M. BARTENER, Paper A-25, First International Conference, Fracture, Vol. 1, Sendai, Japan (1965).
18. D. J. GREEN, P. S. NICHOLSON and J. D. EMBURY, "Fracture Mechanics of Ceramics", Vol. 2, edited by R. C. Bradt *et al.* (Plenum Press, New York, 1974) p. 541.
19. D. J. GREEN, PhD Thesis, McMaster University, Hamilton, Ontario, Canada (1976).
20. K. D. KINGERY, "Introduction to Ceramics" 3rd edn. (Academic Press, New York, 1976).
21. R. G. HOAGLAND, J. D. EMBURY and D. J. GREEN, *Scripta Met.* 9 (1975) 907.
22. F. F. LANGE, *Phil. Mag.* **16** (1967) 761.
23. S. M. OHLBERG, H. R. GELOB and C. M. HALLABAGH, *J. Amer. Ceram. Soc.* 45 (1962) 61.
24. F. F. LANGE, *ibid* 54 (1971) 614.
25. *Idem, Phil. Mag.* 22 (1970) 983.
26. R. B. THOMSON, *Ann. Rev. Mater. Sci.* 3 (1973) 31.
27. A. G. EVANS, *Phil. Mag.* **26** (1979) 1327.
28. J. N. GOODIER, *J. Appl. Mech.* 1 (1933) 39.
29. A. K. KHAUND, V. D. KRSTIC and P. S. NICHOLSON, *J. Mater. Sci.* 12 (1977) 2269.
30. D. J. GREEN, P. S. NICHOLSON and J. D. EMBURY, *ibid* 12 (1977) 987.
31. S. SAHU and L. J. BROUTMAN, *Polymer Eng. Sci.* 12 (1972) 91.
32. D. F. WEIRAUCH, *Amer. Ceram. Soc. Bull.* 57 (1978) 420.
33. V. WEISS, ASME Paper no. 62, WA-270 (1962).

Received 18 May and accepted 10 July 1979.